LIMNOLOGY
and
OCEANOGRAPHY: METHODS

Limnol. Oceanogr.: Methods 8, 2010, 363–375

A low-cost automated trap to measure bubbling gas fluxes

Charuleka Varadharajan, Richard Hermosillo, and Harold F. Hemond*
Department of Civil and Environmental Engineering, Building 48, Massachusetts Institute of Technology, Cambridge, Massachusetts 02139

Abstract

We describe a trap that can be used for automated, high temporal resolution measurement of ebullition fluxes in aquatic environments. The trap comprises a submerged cone connected to a transparent PVC pipe that serves as a collection chamber. A differential pressure sensor at the top of the pipe measures the pressure caused by gas accumulation in the chamber. The sensor circuit consists of low-power electronics and can function for longer than 6 months on two high-capacity AA lithium batteries. The circuit, batteries, and a commercial data logger that records the measurements are enclosed in a custom-made, 10-cm diameter waterproof housing. The trap is designed to be fabricated economically and easily so that many units can be deployed for greater spatial coverage. We have used several of these automated traps to measure bubbling fluxes at a lake, and have collected data continuously at a resolution of 5 or 10 min over 6 months.

Bubbling is an important mechanism for the release of gases to the atmosphere from both freshwater and marine ecosystems. In particular, significant quantities of methane, a powerful greenhouse gas, can be released from sediments to the atmosphere through ebullition (e.g., Hornafius et al. 1999; Glaser et al. 2004; Walter et al. 2007). Ebullition can also serve as a transport mechanism for other volatile species such as nitrogen, hydrogen, carbon dioxide, radon, and hydrogen sulfide (e.g., Martens and Chanton 1989; Chanton and Whiting 1995; Higgins et al. 2008).

Ebullition is a difficult process to quantify, because it is highly variable at several temporal and spatial scales (Fechner-Levy and Hemond 1996; Ostrovsky 2003; Leifer et al. 2004; Walter et al. 2006). Considerable amounts of gas are often emitted during occasional, short-lived bubbling episodes. For example, large, rare emission events lasting for about 30 s have been observed in Siberian lakes (Walter et al. 2006), whereas bubbling events in hydrocarbon seeps have been identified to occur on the scale of a few minutes (Greinert 2008). At the Upper Mystic Lake in Massachusetts, U.S.A, we have observed bubble patches at the lake surface having lifetimes between 1 and 10 min. Ebullition has also been observed to vary seasonally, with higher release occurring during early spring, late summer, and early fall (e.g., Wilson et al. 1989; Casper et al. 2000). Bubbling fluxes tend to increase when there is a decrease in atmospheric pressure (Mattson and Likens 1990; Fechner-Levy and Hemond 1996; Kellner et al. 2006) or a lowering of water level (Chanton et al. 1989; Boles et al. 2001), but the sequence of events that leads to increased ebullition is not well understood.

Bubbling fluxes are typically measured using one of two types of collection chambers (Chanton and Whiting 1995). One method uses chambers filled with air that float on the water surface; fluxes are calculated by measuring the change in concentration of a gas within the chamber over a period. Automated versions of this type of device continuously pump the air from the chamber through an infrared analyzer to obtain methane concentrations, and have been used in several ebullition studies in wetlands (e.g., Sebacher and Harriss 1982; Crill et al. 1988; Bäckstrand et al. 2008; Mastepanov et al. 2008). However, such chambers measure the sum of diffusive and ebullitive fluxes, which then need to be separated by other analyses, and also are problematic to deploy in deep, aquatic environments. A second type of flux chamber consists of a submerged, inverted funnel that traps bubbles and delivers the gas to a collection chamber (e.g., Casper et al. 2000; Huttunen et al. 2001). In such devices, ebullition fluxes are calculated from the volume of gas that accumulates in the

*Corresponding author: Lawrence Berkeley National Lab, 1 Cyclotron Road, Berkeley, California 94720.

Acknowledgments

This work was supported by NSF Doctoral Dissertation Research Grant 0726806, NSF EAR 0330272, a GSA Graduate Student Research Grant and MIT Martin, Linden and Ippen fellowships. Emanuel Borja and Alexandra Patricia Tcaciuc were funded by the MIT and Martin UROP programs and assisted with the fabrication and testing of equipment and with collection of field data. The authors thank the personnel at the MIT Edgerton and Chemistry machine shops for invaluable help with trap design and fabrication, Amy Mueller for assistance with circuit design and troubleshooting, as well as Phil Gschwend and the anonymous reviewers for comments on the manuscript.

DOI 10.4319/lom.2010.8.363

chamber, while bubble composition is typically determined by gas chromatographic analysis after withdrawing the gas from the chamber via syringes.

Most reported ebullition measurements are based on manually tended funnel-type traps that were deployed either for short periods of time and sampled with relatively high frequency (e.g., Martens and Klump 1980; Bartlett et al. 1988; Keller and Stallard 1994), or for long periods with low sampling frequency (e.g., Mattson and Likens 1990; Huttunen et al. 2001). In the former case, major episodes of bubbling may be missed entirely, leading to inaccurate estimates of long-term fluxes. In the latter case, the timing of bubbling events remains unknown within each sampling period. In a long-term study of ebullition fluxes, Walter et al. (2006) deployed 25 traps in Siberian lakes for over 14 months, and collected frequent manual measurements over summer and winter; however their highest sampling resolution was twice a day. Ultimately, long-term measurement with high sampling frequency, as well as adequate spatial density, is necessary to test hypotheses regarding the magnitude, spatiotemporal variability, and mechanisms of bubbling. However, the collection of such data are not practical over long deployment periods without automation. Automation can also help in monitoring fluxes during periods of time or at locations where site conditions render manual field measurements difficult.

An automated funnel-type trap equipped with a differential pressure sensor has previously been used to measure gas fluxes in marine hydrocarbon seeps (Washburn et al. 2001; Clark et al. 2009), although we are unaware of any long-term or extensive deployments of this type of trap. The electronic setup in the device also appears to be expensive, bulky, and time-consuming to build. More recently, acoustic techniques have been used for automated measurement of ebullition (e.g., Greinert and Nutzel 2004; Ostrovsky et al. 2008). While these methods have spatial resolutions in the order of tens to hundreds of meters, they are expensive in terms of cost and power to deploy at several sites. Furthermore, the gas content of bubbles cannot be directly determined, and additional data processing has to be done to estimate methane fluxes to the atmosphere because not all bubbles reach the water surface (McGinnis et al. 2006). Other methods, such as ground penetrating radar (Comas et al. 2007), resistivity (Slater et al. 2007), and GPS measurements of surface deformations (Glaser et al. 2004), have been used for automated measurements of methane ebullition in peatlands; however these cannot be used for long-term monitoring of bubble fluxes in aquatic systems such as lakes, rivers, and ponds.

In this paper, we present a design for an inexpensive, but sufficiently accurate, low-power, automated instrument that uses a differential pressure sensor to measure the volume of bubbled gas as it accumulates in a flux chamber. The design emphasizes not only high sampling frequency but also low cost and ease of construction, in order that an adequate number of units can be deployed to characterize both temporal and spatial variation in bubbling. The device can also be readily adapted to monitor other situations where a pressure differential is of interest. For example, at our field site, we adapted one unit to continuously measure the water level of the lake by repackaging the same electronics in a slightly different enclosure.

Materials and procedure

Trap design—The bubble trap consists of a cone attached to a transparent PVC pipe that functions as a collection chamber in which gas can accumulate (Fig. 1). The bubble collection funnel is made by rolling a sheet of 28-gauge galvanized steel, cut from a pattern, into a cone of diameter 0.5 m and approximate height of 0.16 m. The cone is painted with hard enamel to keep the surface smooth and to minimize corrosion. The seam of the cone is either fastened with blind rivets or spot welded, and sealed with epoxy adhesive and silicone sealant to prevent gas leakage as well as to create a smooth edge on the inside of the cone.

The gas collection chamber is a length of transparent, nominal 1/2 inch (1.27 cm) or 3/4 inch (1.9 cm) schedule 40 PVC pipe. Narrow pipe diameters were chosen to limit the area of the gas-water interface, and hence the amount of methane potentially lost through diffusion to the water column, as well as to increase the sensitivity of the device. Pipe lengths varied from 30 cm to 1 m, and can be modified according to the flux expected at the deployment location. The pipe is marked in 1-cm intervals; thus the height of bubbled gas accumulating in the chamber can be read manually, providing a means for in-field calibration checks.

The collection chamber is connected to the cone through a fitting made from a 5-cm slice of a 2.75 inch (7 cm) diameter PVC rod. A hole (of diameter 2.14 cm [27/32 inch] for the nominal 1/2 inch pipe; 2.7 cm [1.063 inch] for the nominal 3/4 inch pipe) is drilled through the center to accept the pipe, which is attached using standard PVC cement. The opposite face of the fitting is machined to an angle of 34° to fit the top of the cone, to which it is fastened using flat head screws, epoxy adhesive, and silicone sealant.

The collection chamber is capped with a nominal 1/4 inch (0.63 cm) 3-way brass ball valve via a PVC pipe connector of the appropriate size. A second port of the 3-way valve is connected to the pressure sensor housing, whereas the third port is sealed with a rubber septum, through which gas can be withdrawn for analysis. The chambers can hold between 200 and 300 mL gas, depending on the PVC pipe dimensions, before the gas begins to overflow into the collection funnel. It is undesirable to have gas fill up in the funnel because it then becomes difficult to accurately measure the gas volume in the chamber and because the rapidly increasing area of the interface between trapped gas and the water column likely enhances gas exchange.

Three nominal 1/4 inch (0.63 cm) PVC pipes, attached to the cone on one end, and to a 0.63 cm by 30 cm by 30 cm

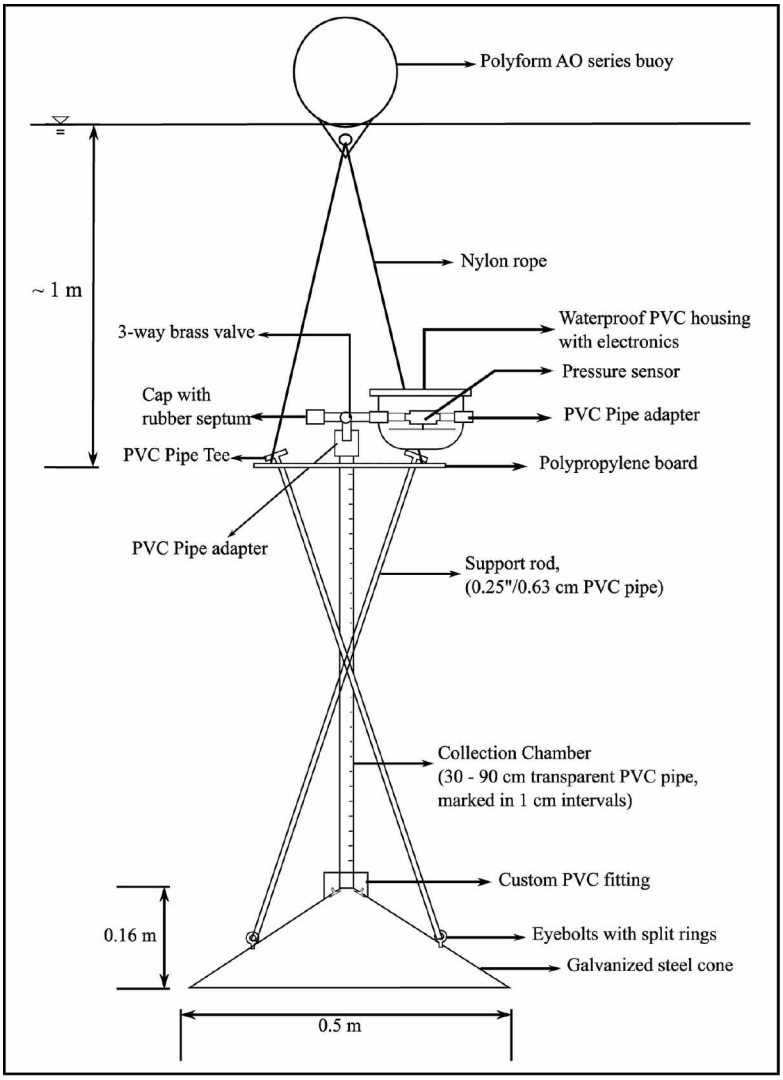

Figure 1. Bubble Trap Assembly.

polypropylene panel on the other end, provide structural stiffness to the assembly. The pipes are arranged to form a cross-bracing that limits flexing caused by wave action. The trap is suspended at a depth of 1 m below the water surface using three 1.5-m ropes connecting the polypropylene board to a polyform A0-series buoy such as is commonly used for marking boat moorings.

Buoys were moored to a concrete block anchor using 1/4 inch (0.63 cm) three-strand nylon rope at several locations with depths ranging from 6 m to 25 m. The entire setup was designed to be unobtrusive, but visible to boat operators, since the traps were deployed in an urban lake that is heavily used for recreational purposes. The total cost of materials for a trap, including the buoy but excluding the electronics, was approximately $85.

Circuit design—The circuit measures the difference in fluid pressure between the top of the gas collection chamber and the outside water column. This pressure is proportional to the height of the gas collected in the chamber and can be converted to a gas volume using the chamber cross-section area.

We used a wet-wet, temperature-compensated differential pressure sensor (26PCAFA6D, Honeywell) that has a manufacturer-specified range of ±1 psi (±6900 Pa). The sensor range is approximately equivalent to ±70 cm of water, and was chosen to maximize the sensitivity of the circuit for the length of a typical collection chamber. The sensor has acceptable accuracy and precision, with a manufacturer-specified stability of ±0.5% FSD over 1 yr, temperature coefficient of ±1% FSD between 0 and 50°C, and linearity and repeatability errors of ±0.25% FSD each (FSD refers to full scale deflection over the operating pressure range of the sensor). A commercial data logger with an inbuilt temperature sensor (H08-002-02, Onset systems) is used to store the final voltage readings from the circuit.

The millivolt pressure sensor output is buffered and amplified to the 0 to 2.5 V data logger range using the circuit shown schematically in Fig. 2. Output from the pressure sensor is applied to an instrumentation amplifier (INA126, Texas

Instruments), which provides a gain of 5 and also presents a high impedance load to the sensor bridge to minimize voltage measurement error. The instrumentation amplifier is followed by an operational amplifier (Op Amp D) set to a gain of 270.

The pressure sensor itself comprises a bridge, which is driven by the difference between the outputs of Op Amp A (3 V) and Op Amp B (2 V). The 1 V excitation voltage for the pressure sensor was chosen instead of the manufacturer's suggested value of 10 V, to keep the power drawn by the sensor to a minimum. A 2.1 V reference, buffered by Op Amp C, creates an offset that results in a slightly positive input to the data logger when the pressure sensor output is zero, biasing it into its allowable input range. The null offsets generated by the circuits range from 0.04 V to 0.35 V; this variation primarily arises from the instrumentation amplifier. The circuit shown in the diagram only uses the 0 to 1 psi range of the pressure sensor and can be modified to use the entire ±1 psi sensor range by changing resistors R5 and R6 to alter the signal reference voltage. The four op-amps are all contained in a single IC device (TLV2404, Texas Instruments).

All electronics other than the self-contained data logger are powered using two 3.6 V, 2.4 A-h AA lithium batteries. A 5 V voltage regulator (LP2952, National Semiconductor) ensures that the supply to the circuit remains constant. Low power circuit elements were selected to keep power consumption to a minimum; the total current drawn from the AA batteries was measured to be 0.41 mA. The circuit can be powered for about 8 months without battery replacement, while the data logger is powered by its own battery that lasts for about a year. Data from the logger can be accessed using a cable connected from a 3.5 mm stereo jack on the logger to the serial port of a PC. The manufacturers' specifications, cost, and power consumption of the electronics are further described in Table 1.

Waterproof housing—The electronic circuitry is enclosed in a housing built from a nominal 4 inch (10.2 cm) schedule 40 PVC pipe cap (Fig. 3). Two 2.18 cm (55/64 inch) holes are drilled on opposite ends of the wall, and nominal 1/4 inch (0.63 cm) schedule 80 PVC, threaded female adapters are cemented into the holes to provide access to the ports of the pressure sensor. The edges around the adapters are sealed to be watertight with epoxy and silicone sealant. The 3-way valve on top of the collection chamber is attached via a nominal 1/4 inch (0.63 cm) brass nipple to one of the adapters, while the second adapter is left open to the water column. The interior

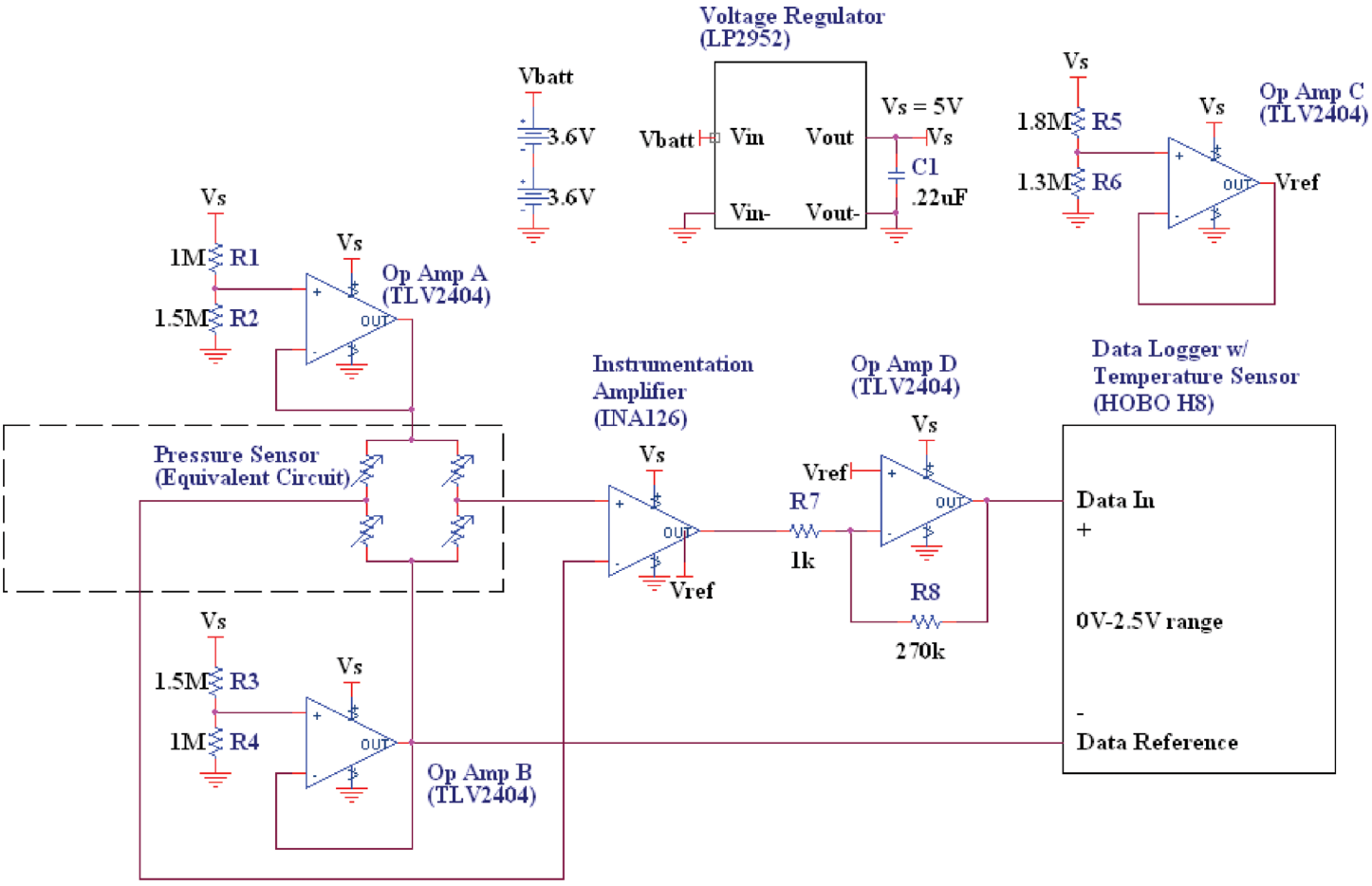

Figure 2. Circuit Diagram.

Table 1. Details of electronics used in the circuit.

Circuit component	Manufacturer	Model	Current consumption	Approximate unit price in 2008
Differential pressure sensor	Honeywell	26PCAFA6D	~0.13 mA	$15–20
Data logger	Onset Systems	HOBO H08-002-02 Temperature/External logger		$45–65
Quad Op-amp chip	Texas Instruments	TLV2404	1 μA	$3
Instrumentation amplifier	Texas Instruments	INA126	175 μA	$3
Voltage regulator	National Semiconductor	LP2952	130 μA for a 1 mA load	$2
2 high capacity 3.6V lithium batteries	Tadiran	TL-5903		$7
PC Board	ExpressPCB			$20

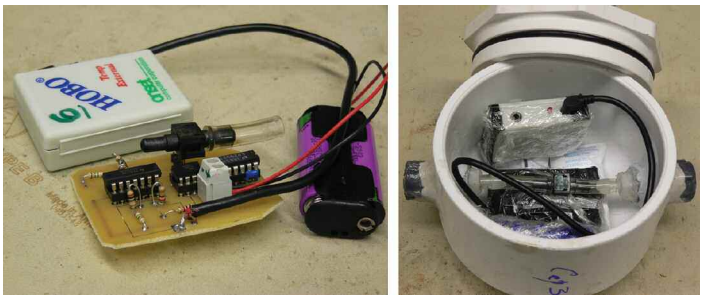

Figure 3. Pictures of circuit (left) and waterproof housing with packaged electronics (right).

ends of the adapters are connected to the pressure sensor ports with short lengths of 3/16 inch (0.48 cm) flexible plastic tubing. The directionality of the pressure sensor is important; the high-pressure port should be connected to the collection chamber end, while the low-pressure port is to be exposed to the water.

The housing is closed with a nominal 4 inch (10.2 cm) schedule 40 PVC pipe plug, cut to a length of 2.5 cm. An O-ring groove, 0.282 cm (0.111 inch) deep and 0.475 cm (0.187 inch) wide, is machined into the plug and fitted with an EPDM O-ring (dash size 244). The plug and groove are chamfered at the edges to create smooth surfaces, and the O-ring is greased before sealing the housing.

The enclosure can be tested for leaks in the laboratory using a vacuum test, in which connections to the sensor are removed and one of the adapters in the housing is plugged to be airtight. The second adapter is attached to a vacuum pump via a tee fitting having a vacuum pressure gage on one end and a ball valve on the other so that vacuum can be retained in the housing once the pump is turned off. In tests, approximately 3700 Pa (28 inches of mercury) vacuum was applied; a leaky housing could be easily detected within a few seconds, whereas a satisfactory seal would allow only a minor pressure increase (order of 100 Pa, or 1 inch mercury) over a 30-min period.

In addition, circuits were assembled in their housings and left overnight in a water bath before deployment; this served as a secondary leak test as well as ensured that the circuits were working correctly. Indicating silica gel desiccant packs were inserted into the housings before deployment in the field. During periods when the housing was being opened frequently for data download, the O-rings had to be replaced in the field about once every 2 to 3 weeks to ensure a watertight seal. However, the housings can be used for autonomous long-term deployment without replacing the O-rings, as demonstrated by the effective seals in 3 devices that were left in the lake from December 2008 to August 2009.

Field deployment and sampling—Gas was collected from the traps for analysis typically every 4 to 13 days. The height of the bubbled gas column was measured before sampling using the markings on the transparent collection chamber. Gas was then withdrawn from the collection chamber into syringes, thus filling the chamber with water. Finally, pressure data were downloaded and the data logger was reset to clear its memory. The data logger can store data for 13.5 days at a measurement interval of 5 min, or proportionally longer with larger measurement intervals.

Modifications made for measuring water level—The circuit described above can also be used to monitor the water level of a lake by measuring the pressure difference between the water column at a fixed point in the lake and the ambient atmospheric pressure. The assembly was modified for this purpose by venting one pressure port to the atmosphere. This can be done, for example, with a 75 cm long nominal 1/4 inch (0.63 cm) schedule 40 PVC pipe. A 90° elbow, with a mesh blocking its open end, was cemented to the top of the pipe to prevent the entry of rainwater, insects, and debris. Also, the pressure sensor direction must be reversed, such that the low-pressure port connects to the atmosphere, and the high-pressure port connects to the water column.

Data reduction and circuit calibration—The height of the gas column in the collection chamber (h_s) was calculated from the voltages recorded by the data logger using calibration curves that were determined in the laboratory for each circuit. The calibration setup involved connecting the tip of a burette to one of the pressure sensor ports through a short length of tubing, while the second sensor port was left open to atmospheric pressure. After removing any air bubbles in the tubing, water was added to the burette at approximately 4 cm height intervals and the corresponding voltage outputs from the circuit, as

recorded by the data logger, were noted in a process adapted from the calibration procedure used by Gardner et al. (2009).

Each circuit was calibrated thrice—first before deployment in the field, second at the end of the field season to check for sensor drift, and finally in a cold room at approximately 5°C to estimate the effect of temperature changes. Measured circuit responses were linear within the 0 to 2.5 V output range, with Pearson correlation coefficients (R^2) greater than 0.99. An inverse linear regression on the calibration data gave slope and offset values that can be used to convert the circuit output voltage to height, h_g in cm.

Slope values varied among calibrations from 27.1 to 29.2 cm/Volt across circuit units, and were within the range expected from the manufacturer's specifications. However, offset values obtained from laboratory calibrations ranged from 1.95 to 12.6 cm among the different circuits from the start to the end of the ~6 month deployment period. Variations in offset were caused due to a combination of sensor and amplifier drift, temperature effects, and seemingly random measurement errors. Thus, to achieve the most accurate data reduction, offsets measured in the laboratory were replaced with field offsets that were based on voltage readings obtained every time the collection chamber was emptied during gas collection.

The equation for conversion of voltage readings to h_g, the gas height in the collection chamber (in cm), is

$$h_g = \bar{m}(V_{out} - \bar{V}_{zero}) \quad (1)$$

where $\bar{m}$ = average slope from laboratory calibrations (cm/Volt), V_{out} = Voltage output recorded on the data logger (Volt), and $\bar{V}_{zero}$ = Average of empty trap voltages measured in the field during the first 1 to 2 h following gas collection (Volt). Voltages from the beginning and end of each sampling interval were also averaged to account for possible short-term drift and temperature effects.

The gas height, h_g, was multiplied by the cross-sectional area of the collection chamber (1.88 cm^2 for nominal 1/2 inch schedule 40 pipes and 3.32 cm^2 for nominal 3/4 inch schedule 40 pipes) to determine the volume of gas present in the trap. It should be noted that actual PVC pipe dimensions can differ from published values, and that using the latter can lead to significant errors in volume calculations. Volumes measured at the 1 m deployment depth of the traps were normalized to 1 atmosphere and 20°C, assuming ideal gas behavior. The normalized volume of gas present in a trap is calculated as:

$$Vol\ (\text{in mL}) = \left(1 + \frac{\rho_{water} g}{P_{atm}} * (1 + 0.01 * h_g)\right) A_c h_g * \frac{293}{T_{trap}} \quad (2)$$

where ρ_{water} is 998 kg/m^3 at 20°C, P_{atm} = 101 kPa, g = 9.8 m/s^2, h_g = height of gas accumulated in the collection chamber (cm) from Eq. 1, A_c = cross-section area of the collection chamber (cm^2), and T_{trap} = temperature recorded by the data logger (°K).

Temperature differences between the water at 1-m depth and the surface, as well as day-to-day barometric pressure and temperature variations, were neglected for purposes of this calculation. Any buoyancy effect caused due to gas accumulating in the collection chamber was also considered to be negligible.

An additional dead volume correction was applied to automated measurements obtained from traps that used a 3/4 inch PVC pipe as the collection chamber. A reducing pipe adapter was cemented to the top of the collection chamber, and multiplying the height of the adapter by the chamber cross-section area led to a volume overestimation of about 9 mL. No correction was applied to automated data from traps with 1/2 inch pipes because the effective diameter of the pipe adapter was nearly the same as the collection chamber diameter, and amounted to a volume difference of ~1 mL.

Manual gas measurements—The volumes obtained using the pressure sensor data were compared with manual gas measurements to verify circuit behavior. Manual volumes were measured in two ways: (1) by recording the total volume of gas collected in syringes while emptying the collection chamber, and (2) by multiplying the gas height in the transparent PVC pipe by the collection chamber cross-section area. Because the height markings on the transparent pipe start below an opaque pipe adapter attached to the top of the collection chamber, the adapter volume (6.5 to 9.5 mL for the 1/2 inch pipe and 12 to 13 mL for the 3/4 inch pipe) has to be added to obtain a final value for the manual volume reading.

The manual volume measurements were, whenever possible, an average of values obtained using both methods. Exceptions were made for instances when no syringe samples were taken or when the gas height reading was hidden by the opaque pipe adapter. The standard deviation (1σ) of readings obtained using the two methods was typically around 1 to 3 mL, depending on the collection chamber dimensions, and was used as an error estimate for the manual measurements.

Assessment

Results—Traps built in this design were continuously deployed from June to November 2008, at as many as 7 stations at any given time (Fig. 4). Data were collected at a resolution of 5 or 10 min (e.g., Fig. 4 inset). Gas volumes measured by properly functioning automated traps were deviant from manual readings by 2 ± 2 mL (1σ) for a total of 130 readings (Fig. 5).

Error budget terms for volumes measured in automated traps—The error estimate for volumes calculated using data obtained from the automated traps includes the effects of sensor drift and temperature on circuit electronics, calibration errors, and possible dead volume errors caused by the inability to quantify the small amount of gas that could be trapped in the fittings at the top of the collection chamber. A control trap was deployed for 4 weeks at a location that had no bubbling, which was determined based on manual measurements collected in 2007. Data obtained at 5-min resolution from this trap was additionally used to estimate the effects of circuit drift, temperature, and wind on empty trap voltages.

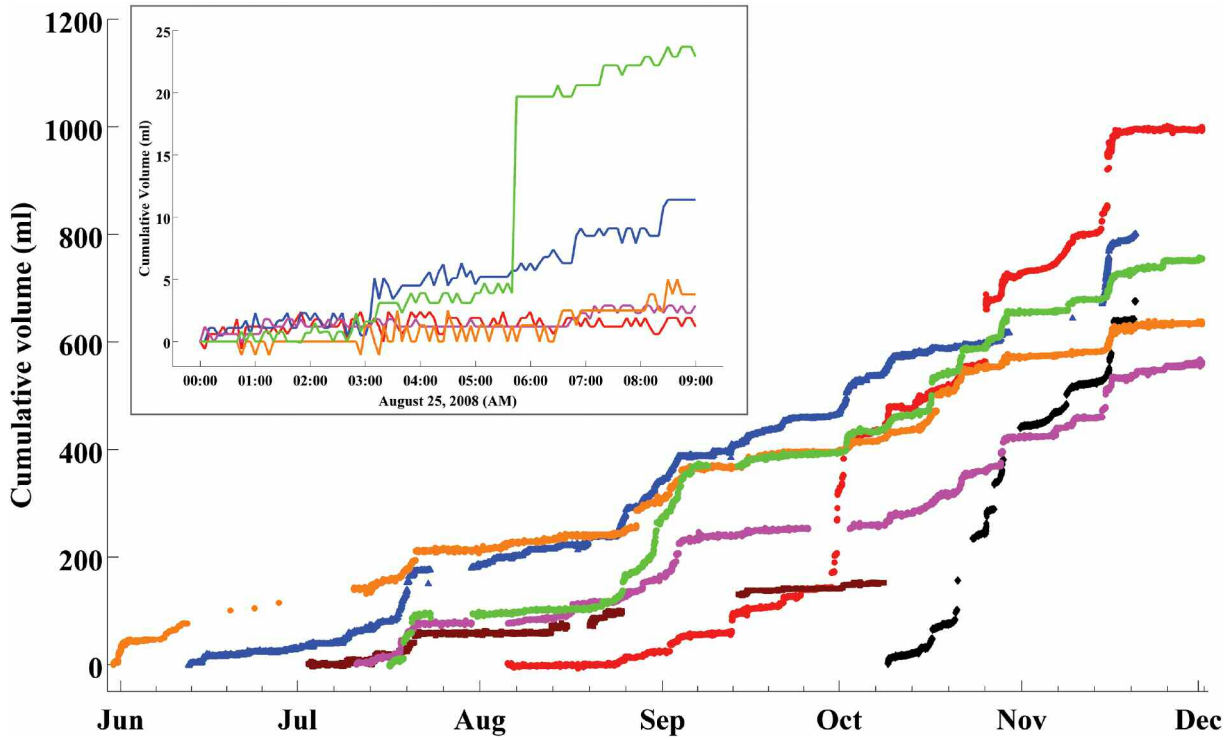

Figure 4. Bubbled gas measured at 5 or 10 minute resolution from June to December 2008 at different sites. (Inset: Close up of data collected between 12 AM and 9 AM on 25 Aug 2008). Cumulative volumes shown are initialized to zero for purposes of comparison. The step edges indicate times when bubbling episodes occurred, leading to an increase in the volume of gas collected by the trap. Note the expanded scale in the inset volumes.

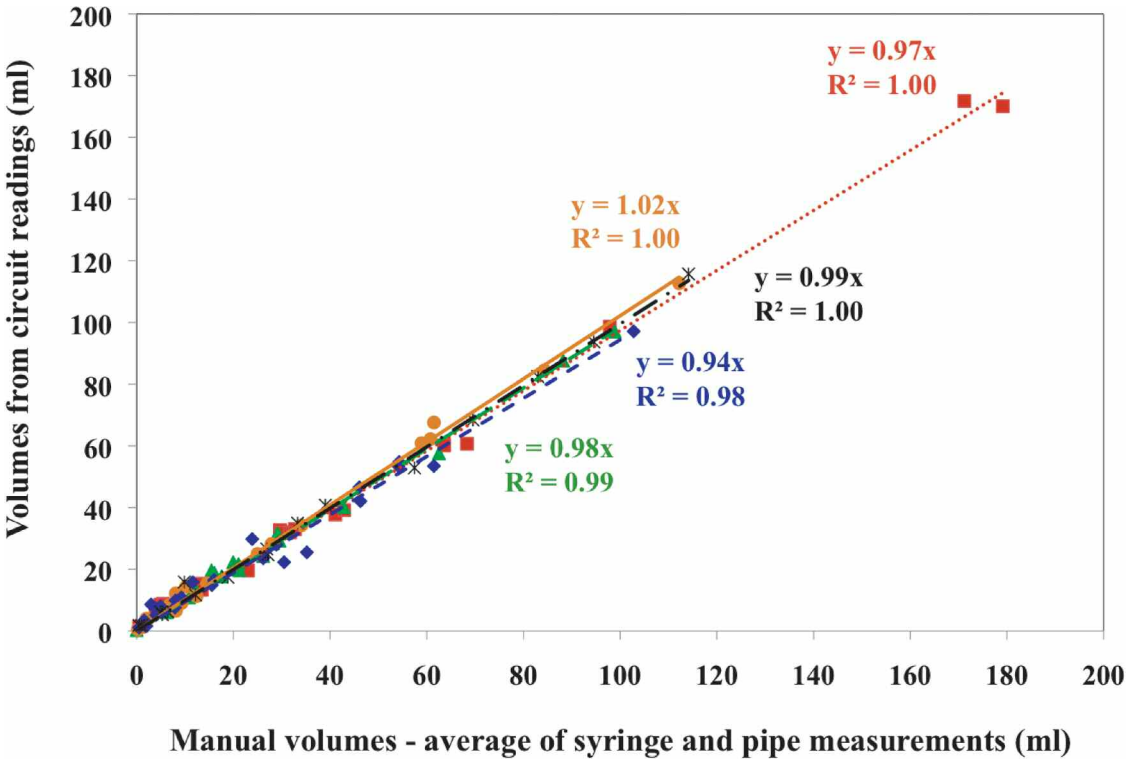

Figure 5. Comparison of volumes obtained from five automated traps with a hundred manual observations collected over 6 months. Volumes shown above are normalized to 1 atm and 20°C.

A root sum squared (RSS) propagation of uncertainty (Kline 1985) can be applied to Eq. 2 to obtain the error in estimated gas volume. The error in collection chamber cross-section area is neglected in the following error budget because the diameters along the length of representative pipe samples, as measured by vernier calipers, were uniform within the readability of the instrument (±0.05 mm). The error caused due to the normalization of gas volume to 1 atm and 20°C is also insignificant. However, an additional term is included to account for dead volume errors, which are on the order of 1–2 mL. The "Δ" in the following equations denotes the standard deviation (1σ) of a term.

The final error in volume, Δ*Vol,* is approximately:

$$\Delta Vol \approx Vol * \sqrt{\left(\frac{\Delta h_g}{h_g}\right)^2 + \left(\frac{\Delta T}{T}\right)^2} \pm Dead\ volume\ error \qquad (3)$$

The error in height (Δh_g) can be calculated as shown in Eq. 4 by applying the RSS propagation of uncertainty to Eq. 1. The height error includes a slope component (Δm), an offset error (ΔV_{zero}), and can also be affected by electronic noise (ΔV_{out}).

$$\Delta h_g \approx \sqrt{\Delta m^2 \left[V_{out}^2 + \bar{V}_{zero}^2\right] + \bar{m}^2 \left[\Delta V_{out}^2 + \Delta V_{zero}^2\right]} \qquad (4)$$

The standard deviation of slopes obtained from all the laboratory calibrations for a sensor unit was used as an estimate of slope error (Δm). Multiple calibrations were done at the start and end of the season, and at normal room temperatures and cold room temperatures. Temperature variations during the calibrations were on the order of 2 to 3°C. Thus results include the effects of calibration procedure error, long-term sensor drift, and changes in temperature. Slope variability between circuits was not considered since each unit was calibrated independently for subsequent data conversion. Slope errors varied from 0.02 cm/Volt (0.02%) to 0.58 cm/Volt (2%) among different units, which is in accordance with the theoretical expected slope error calculated using the pressure sensor manufacturer's specifications (Varadharajan 2009).

The offset error (ΔV_{zero}) determined from field measurements includes the effects of short-term voltage drift and temperature fluctuations. It also includes random volume errors caused either due to incomplete flushing of gas from the collection chamber, or due to possible unknown, irretrievable gas quantities remaining in the trap after gas sampling. The offset error at any point in time is calculated as the standard deviation (1σ) of the two nearest empty trap voltages. The standard deviations mostly ranged between 0 and 30 mV; empty trap voltages deviant by more than 30 mV from the average value were considered outliers and excluded from all calculations. These outliers occurred on 10 of 125 occasions, and could typically be attributed to excessive residual gas due to incomplete sampling of the trap, or to bubbling that occurred between the time of sampling and the start of data collection.

Electronic noise (V_{out}) of up to ±12 mV was observed between adjacent logged values of some circuits when the pressure difference and the ambient temperature were held constant. Most (10 mV) of the noise can be attributed to the precision error of the data logger. The various circuit elements (voltage regulator, amplifiers, and pressure sensor) can also contribute to noise. Electronic noise can be greatly reduced by increasing the sampling frequency and averaging a larger number of measurements over a given sampling period.

Typical values of slope (28 ± 0.5 cm/Volt), offset (0.15 ± 0.015 Volt), and smoothed electronic noise (0.003 Volt using a 1-h moving average filter) can be inserted into Eq. 4 to calculate the error in gas height. The error for a 70 cm gas column, corresponding to a maximum output voltage of 2.485 ± 0.015 V, is 1.4 cm (~2%).

$$\Delta h_g = \sqrt{(0.5)^2\left[2.485^2 + 0.15^2\right] + (28)^2\left[2 * \left((0.003)^2 + (0.015)^2\right)\right]} = \pm 1.4 \text{ cm} \qquad (5)$$

The error in volume is calculated using Eq. 3, and assumes an uncertainty of 2 mL for random dead volume effects. The errors in temperatures recorded by the data logger (1 to 2°C) are negligible in comparison to the height error. The estimated volume error is on the order of 3 to 5 mL for the nominal 1/2 inch PVC pipe and 4 to 6 mL for the nominal 3/4 inch PVC pipe. The actual error will depend on the volume of gas collected in the trap, with a minimum 3-mL uncertainty present for an empty trap.

Effect of changes in temperature—The seasonal variation in water temperatures in the Upper Mystic Lake is on the order of 20°C; fluxes are normalized to 20°C to account for temperature effects on gas volumes (as in Eq. 2). Keeping the traps underwater in the field minimizes temperature effects; the maximum temperature change recorded between sampling intervals within the electronics casing was 6°C.

Additional tests were conducted to determine temperature effects on circuit output voltages in the absence of a pressure differential. Large, abrupt temperature variations were found to affect circuit voltages, even when no pressure was applied across the ports. This effect was quantified as a temperature coefficient calculated from the shift in voltage when a circuit at room temperature (20 to 25°C) was moved to a cold room (~5°C), with both sensor ports exposed to ambient air pressure (Fig. 6). In laboratory tests, the voltages of five circuits were measured at normal room temperatures for 2 d, followed by 2 d in the cold room, and finally for a day back at normal room temperature. Voltages were strongly correlated with temperatures during the transition from room temperature to 5°C and vice versa, which occurred within less than half an hour. Temperature coefficients ranged from –1 mV/°C to –3.4 mV/°C in all but one circuit, which had a coefficient of –11 mV/°C. The circuits were also tested in a refrigerator (–5 to 5°C) to mimic winter conditions, and measured temperature coefficients fell within the range of ±2.5 mV/°C.

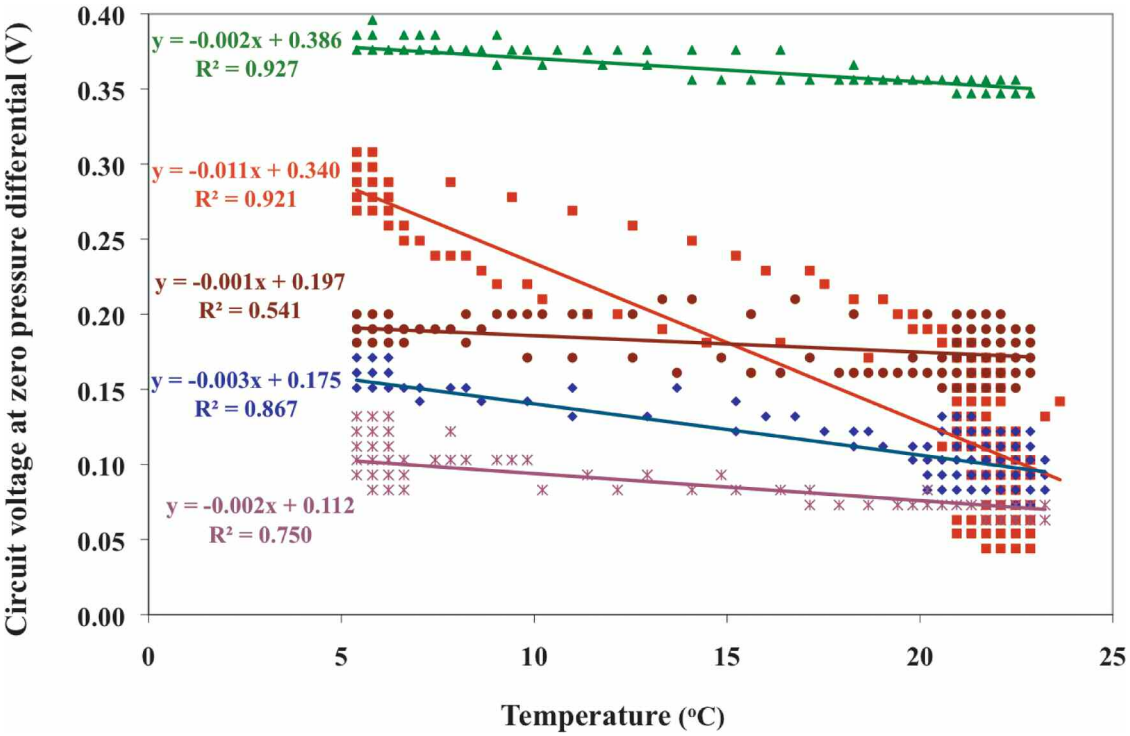

Figure 6. Temperature coefficients of five sample circuits measured in laboratory tests. Data were recorded at 2-minute intervals.

However, zero-pressure differential output voltages were poorly correlated with temperatures when the circuits were operated at normal room temperatures. The same was true in the case of the field-deployed control trap, where temperature changes were gradual and on the order of 2 to 5°C. Thus, although the effect of temperature on output voltages is in concept a systematic error, it was treated as a random error for data reduction. The magnitude of the temperature effect is already included in the standard deviation of field offsets observed between trap samplings, along with the effects of short-term drift and other random errors (i.e., ΔV_{zero} in Eq. 4). Temperature effects do not have to be separately calculated in the error budget, unless the traps are subject to large, sudden temperature changes between sampling intervals.

Independent lab tests confirmed that the data logger units were not significantly affected by changes in temperature. The temperature sensor in the data logger has a published accuracy of ±0.8°C, and resolution of ±0.4°C under ambient conditions.

Effect of wind and waves—The voltages recorded by the automated traps include the effect of pressure fluctuations resulting from buoy movement due to wind and associated wave action. This noise is not included in the ΔV_{out} or ΔV_{zero} terms in Eq. 4, but was estimated by comparing voltages recorded at the control trap with wind speeds obtained from an anemometer installed on a buoy in the middle of the lake (Fig. 7). Almost no noise was observed during periods when the wind speed was below 3 kmph; the typical noise was on the order of ±10 mV, which corresponds to a gas column height of ~3 mm, during moderate wind conditions. Increases in the height of the gas column during bubbling episodes are at least an order of magnitude larger than the typical wind noise; thus the effect of wind is mainly apparent during periods when gas does not accumulate in the trap. A simple moving average filter can be used to smooth the automated trap data to eliminate wind effects before calculating gas fluxes.

Other tests—Laboratory tests showed that the pressure sensor could drift for a short period immediately after the applied pressure on a port is removed (e.g., after servicing the traps in the field). This effect was especially apparent when rapid gas accumulation during the preceding deployment had caused the pressure sensor to go out of its 1 psi range for more than a few hours. The circuit voltage in this situation decreased rapidly and had a recovery period of approximately 1 h; thus voltage readings from the first hour after trap servicing were dropped from field offset calculations in instances where such behavior was suspected. Any possible effect of hysteresis on the pressure sensor readings was neglected, because the pressure only increases during gas accumulation.

The variability in empty-trap voltages was used to monitor the long-term stability of the pressure sensor; standard deviations in voltages were typically less than 30 mV throughout the period of deployment. However, empty-trap voltages could drift by as much as 0.1 V during the first week of deployment in some traps, after which the voltages stabilized for the remainder of the season (Varadharajan 2009).

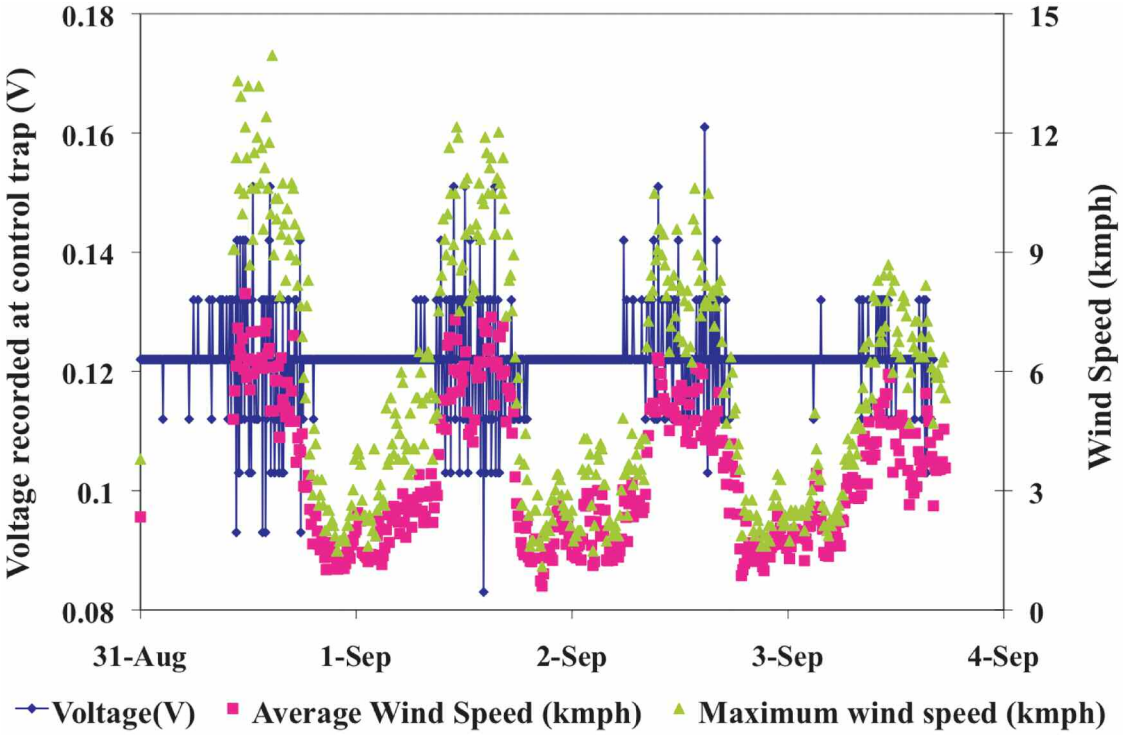

Figure 7. Effect of wind/wave action on circuit output voltage at a control trap for a sample 4 day period. Voltages measured by the circuit at a resolution of 5 minutes were compared against 10-minute wind speed data obtained from an anemometer located close to the control trap.

The possible extent of methane loss due to dissolution during trap deployment was tested by injecting 48 ± 2 mL of pure methane gas into a trap. The trap was left for 2 d in the lake at a site where no bubbling had been observed during the 2007 field season. 46 ± 2 mL gas, which contained 94% methane and approximately 0.1% oxygen, was recovered. The low oxygen concentration of the recovered gas sample indicates that the decrease in methane was not caused due to leakage of air into the chamber. Gas samples were injected and collected from the traps using glass syringes, which were stored underwater. Laboratory analysis commenced within 24–48 h of collection and was done on a flame ionization detector (FID) gas chromatograph (Perkin Elmer 3920B) for methane and on a thermal conductivity detector (TCD) gas chromatograph for oxygen (F&M Scientific Corporation). Laboratory tests of samples and standards stored underwater in glass syringes showed ~1% to 3% methane loss after 7 d; some of the methane may have also been lost during the transfer of gas into the syringes.

Discussion

Bubbling at the Upper Mystic Lake is an episodic process, where high flux periods with gas release rates on the order of hundreds to thousands of mL/(m^2-day) are interspersed with low flux conditions where rates average only tens of milliliters of gas/(m^2-day). The automated bubble trap described in this article can be used both to measure ebullition events on the scale of minutes, and to continuously monitor fluxes on a long-term (months) basis. The cumulative volumes logged by these traps over a 4- to 6-month deployment intervals matched the cumulative sum of manual gas volume measurements within 4%. Deployed in a water-level recording mode, a modified device matched readings from a commercial water level sensor (Model 3001 Levelogger Gold, Solinst) within 1%. To our knowledge, there has been no previous study that has measured freshwater bubbling fluxes over a comparable period with this level of temporal resolution.

A comparison of the data from the automated traps against the measured total hydrostatic pressure signal (i.e., the sum of water column height plus barometric pressure) showed that falling hydrostatic pressures were associated with the onset of synchronous lake-wide bubbling episodes, whereas hydrostatic pressure increases led to an almost immediate cessation of bubbling (e.g., Fig. 8). This is consistent with previous observations of synchronized bubbling episodes in other lakes that were associated with low air pressure events (Mattson and Likens 1990; Casper et al. 2000). Significant negative correlations ($p < 0.05$) were found between daily ebullition fluxes and hydrostatic pressure (Table 2) measured between June and December 2008 at all traps except one that had very low fluxes during its period of automated measurement (Trap 4). However, the low R^2 values indicate that the relationship between hydrostatic pres-

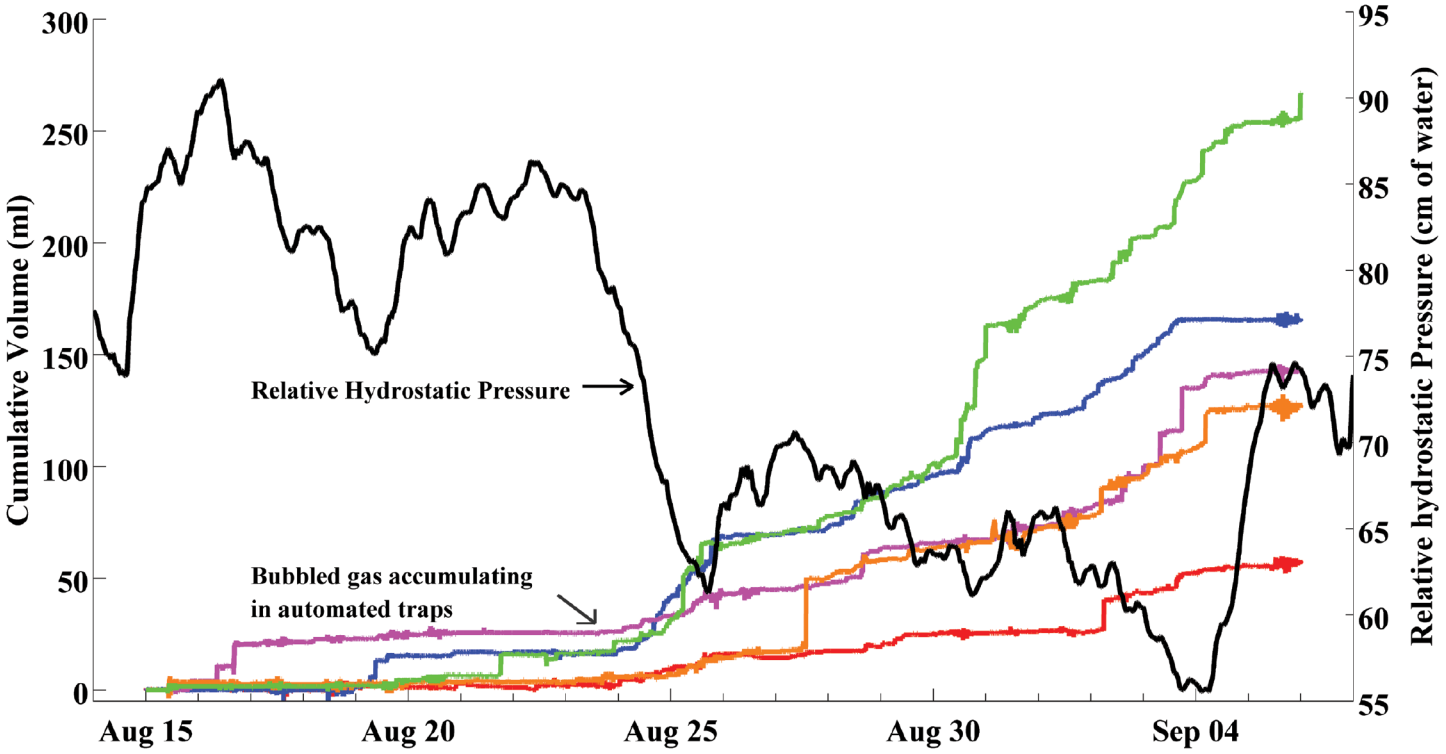

Figure 8. Falling hydrostatic pressures triggered synchronized bubbling episodes at the Upper Mystic Lake (e.g. 25 Aug 2008), while pressure increases caused bubbling to stop (e.g. 4 Sep 2008). Cumulative volumes shown are initialized to zero for purposes of comparison. Noise caused due to wind (e.g., 5 Sep 2008) can be eliminated with a 1-hour moving average filter.

Table 2. Correlation coefficients (R) and statistical significance levels (p) for daily trap fluxes (mL m^{-2} d^{-1}) versus relative hydrostatic pressure (cm of water).

	Period of deployment (2008)	R (p)
Trap 1	5 Aug–1 Dec	–0.4 (0.00)
Trap 2	9 Oct–20 Nov	–0.5 (0.00)
Trap 3	12 Jun–29 Oct, 14 Nov–20 Nov	–0.5 (0.00)
Trap 4	2 Jul–25 Aug, 13 Sep–8 Oct	–0.1 (0.31)
Trap 5	10 Jul–1 Dec	–0.5 (0.00)
Trap 6	30 May–12 Jun, 10 Jul–1 Dec	–0.5 (0.00)
Trap 7	16 Jul–1 Dec	–0.6 (0.00)
Control trap (no bubbling)	5 Aug–3 Sep	–0.1 (0.68)

sure and ebullition fluxes is not linear, and that bubbling could possibly be triggered by other mechanisms such as inter-episode gas buildup within the sediments. Thus, in addition to precisely identifying the timing of bubbling episodes, the high-temporal resolution data from the automated traps can also be used to gain insight into the processes that can cause ebullition.

However the trap cannot be used, without significant alteration to its design, to measure extremely high bubbling fluxes present in locations such as the hotspots and point sources identified by Walter et al. (2006), where fluxes often exceeded 10000 mL m^{-2} d^{-1}. The same study found that the bubbling at these locations contributed to ~75% of the total methane release from their lakes, and that low-intensity background ebullition, as measured by randomly placed traps, comprised a small fraction of the total flux. Random deployment of traps would likely underestimate bubble fluxes, if discrete seeps with small spatial footprints but extremely high ebullition fluxes were present. The design of a mooring scheme, which in our case results in a watch circle of ~10 m radius, could in some cases, also affect observed temporal variability in fluxes.

Comments and recommendations

The trap described here can be adapted to measure a varying range of ebullition fluxes by altering the diameter and length of the collection chamber. However, since the design proposed in this article relies on the height of the gas in the collection chamber as an indicator of gas flux, it is advantageous to have a high aspect ratio to maximize sensitivity and minimize absolute volume errors. Narrow pipe diameters also limit the surface area available for gas-exchange within the collection chamber. For higher volume measurements, a larger diameter PVC pipe could be inserted into, for example, the bottom half of the collection chamber by means of reducing adapters (e.g., a commercially available nominal 2 inch to 3/4 inch PVC pipe coupling). This would increase the gas capacity of the chamber (to ~1500 mL in the above example), while maximizing the sensitivity of the circuit under low-flux conditions. At locations where extremely large volumes of ebullition need to be measured, an electronic valve could be fitted at the top of the collection chamber to automatically release gas when it crosses a threshold, as implemented in Washburn et al. (2001). For situations where greater sensitivity is desired, an auto-zeroing technique that completely eliminates offset errors using a 3-way solenoid valve could be used as shown in Gardner et al. (2009).

In situations where the trap can only be partially submerged due to logistical reasons (for example, in a shallow pond or ice-cover), air from the collection chamber could be removed at the beginning of deployment by applying a mild suction, for example using a syringe. The trap and circuit design described above could also be used with various modifications to the mooring system, as long as some part of the cone is kept underwater. However, circuits deployed above water will probably be subject to increased variations in temperature and might require the application of temperature corrections.

References

Bäckstrand, K., P. M. Crill, M. Mastepanov, T. R. Christensen, and D. Bastviken. 2008. Total hydrocarbon flux dynamics at a subarctic mire in northern Sweden. J. Geophys. Res. 113:G03026 [doi:10.1029/2008JG000703].

Bartlett, K. B., P. M. Crill, D. I. Sebacher, R. C. Harriss, J. O. Wilson, and J. M. Melack. 1988. Methane flux from the central Amazonian floodplain. J. Geophys. Res. 93(D2):1571-1582 [doi:10.1029/JD093iD02p01571].

Boles, J. R., J. F. Clark, I. Leifer, and L. Washburn. 2001. Temporal variation in natural methane seep rate due to tides. Coal Oil Point area, California. J. Geophys. Res. 106(C11):27077-27086 [doi:10.1029/2000JC000774].

Casper, P., S. C. Maberly, G. H. Hall, and B. J. Finlay. 2000. Fluxes of methane and carbon dioxide from a small productive lake to the atmosphere. Biogeochemistry 49:1-19 [doi:10.1023/A:1006269900174].

Chanton, J. P., C. S. Martens, and C. A. Kelley. 1989. Gas transport from methane-saturated, tidal freshwater and wetland sediments. Limnol. Oceanogr. 34:807-819 [doi:10.4319/lo.1989.34.5.0807].

———, and G. J. Whiting. 1995. Trace gas exchange in freshwater and coastal marine environments: ebullition and transport by plants, p. 98-125. *In* P. A. Matson and R. C. Harriss [eds.], Biogenic trace gases: Measuring emissions from soil and water. Blackwell Science.

Clark, J., L. Washburn, and K. Schwager Emery. 2009. Variability of gas composition and flux intensity in natural marine hydrocarbon seeps. Geo-Mar. Lett. [doi:10.1007/s00367-009-0167-1].

Comas, X., L. Slater, and A. Reeve. 2007. In situ monitoring of free-phase gas accumulation and release in peatlands using ground penetrating radar (GPR). Geophys. Res. Lett. 34:L06402 [doi:10.1029/2006GL029014].

Crill, P. M., and others. 1988. Tropospheric methane from an Amazonian floodplain lake. J. Geophys. Res. 93:1564-1570 [doi:10.1029/JD093iD02p01564].

Fechner-Levy, E. J., and H. F. Hemond. 1996. Trapped methane volume and potential effects on methane ebullition in a northern peatland. Limnol. Oceanogr. 41:1375-1383 [doi:10.4319/lo.1996.41.7.1375].

Gardner, A. T., H. N. Karam, A. E. Mulligan, C. F. Harvey, T. R. Hammar, and H. F. Hemond. 2009. A differential pressure instrument with wireless telemetry for in-situ measurement of fluid flow across sediment-water boundaries. Sensors 9:404-429 [doi:10.3390/s90100404].

Glaser, P. H., and others. 2004. Surface deformations as indicators of deep ebullition fluxes in a large northern peatland. Global Biogeochem. Cycles 18:GB1003 [doi:10.1029/2003GB002069].

Greinert, J. 2008. Monitoring temporal variability of bubble release at seeps: The hydroacoustic swath system GasQuant. J. Geophys. Res. 113:C07048 [doi:10.1029/2007JC004704 ER].

——— and B. Nützel. 2004. Hydroacoustic experiments to establish a method for the determination of methane bubble fluxes at cold seeps. Geo-Mar. Lett. 24:75-85 [doi:10.1007/s00367-003-0165-7].

Higgins, T., J. McCutchan, and W. Lewis. 2008. Nitrogen ebullition in a Colorado plains river. Biogeochemistry 89:367-377 [doi:10.1007/s10533-008-9225-4].

Hornafius, J. S., D. Quigley, and B. P. Luyendyk. 1999. The world's most spectacular marine hydrocarbon seeps (Coal Oil Point, Santa Barbara Channel, California) - Quantification of emissions. J. Geophys. Res. 104(C9):20703-20711 [doi:10.1029/1999JC900148].

Huttunen, J. T., K. M. Lappalainen, E. Saarijärvi, T. Väisänen, and P. J. Martikainen. 2001. A novel sediment gas sampler and a subsurface gas collector used for measurement of the ebullition of methane and carbon dioxide from a eutrophied lake. Sci. Total Environ. 266:153-158 [doi:10.1016/S0048-9697(00)00749-X].

Kline, S. J. 1985. The purposes of uncertainty analysis. J. Fluids Eng. 107:153-160 [doi:10.1115/1.3242449].

Keller, M., and R. F. Stallard. 1994. Methane emission by bubbling from Gatun Lake, Panama. J. Geophys. Res. 99(D4):8307-8319 [doi:10.1029/92JD02170].

Kellner, E., A. J. Baird, M. Oosterwoud, K. Harrison, and J. M. Waddington. 2006. Effect of temperature and atmospheric pressure on methane (CH4) ebullition from near-surface peats. Geophys. Res. Lett. 33:L18405 [doi:10.1029/2006GL027509].

Leifer, I., J. R. Boles, B. P. Luyendyk, and J. F. Clark. 2004. Transient discharges from marine hydrocarbon seeps: spatial and temporal variability. Environ. Geol. 46:1038-1052 [doi:10.1007/s00254-004-1091-3].

Martens, C. S., and J. V. Klump. 1980. Biogeochemical cycling in an organic-rich coastal marine basin-I. Methane sediment-water exchange processes. Geochim. Cosmochim. Acta. 44:471-490 [doi:10.1016/0016-7037(80)90045-9].

———, and J. P. Chanton. 1989. Radon as a tracer of biogenic gas equilibration and transport from methane-saturated sediments. J. Geophys. Res. 94(D3):3451-3459 [doi:10.1029/JD094iD03p03451].

Mastepanov, M., C. Sigsgaard, E. J. Dlugokencky, S. Houweling, L. Ström, M. P. Tamstorf, and T. R. Christensen. 2008. Large tundra methane burst during onset of freezing. Nature. 456:628-630 [doi:10.1038/nature07464].

Mattson, M. D., and G. E. Likens. 1990. Air pressure and methane fluxes. Nature. 347:718-719 [doi:10.1038/347718b0].

McGinnis, D. F., J. Greinert, Y. Artemov, S. E. Beaubien, and A. Wüest. 2006. Fate of rising methane bubbles in stratified waters: How much methane reaches the atmosphere? J. Geophys. Res. 111:C09007 [doi:10.1029/2005JC003183].

Ostrovsky, I. 2003. Methane bubbles in Lake Kinneret: Quantification and temporal and spatial heterogeneity. Limnol. Oceanogr. 48:1030-1036.

———, D. F. McGinnis, L. Lapidus, and W. Eckert. 2008. Quantifying gas ebullition with echosounder: The role of methane transport by bubbles in a medium-sized lake. Limnol. Oceanogr. Methods. 6:105-118.

Sebacher, D. I., and R. C. Harriss. 1982. A system for measuring methane fluxes from inland and coastal wetland environments. J. Environ. Qual. 11:34-37 [doi:10.2134/jeq1982.11134x].

Slater, L., X. Comas, D. Ntarlagiannis, and M. R. Moulik. 2007. Resistivity-based monitoring of biogenic gases in peat soils. Water Resour. Res. 43:W10430 [doi:10.1029/2007WR006090].

Varadharajan, C. 2009. Magnitude and spatio-temporal variability of methane emissions from a eutrophic freshwater lake. Ph.D. thesis, Massachusetts Institute of Technology.

Walter, K. M., S. A. Zimov, J. P. Chanton, D. Verbyla, and F. S. Chapin III. 2006. Methane bubbling from Siberian thaw lakes as a positive feedback to climate warming. Nature 443:71-75 [doi:10.1038/nature05040].

———, L. C. Smith, and F. S. Chapin III. 2007. Methane bubbling from northern lakes: present and future contributions to the global methane budget. Philos. Trans. R. Soc. A. 365:1657-1676 [doi:10.1098/rsta.2007.2036].

Washburn, L., C. Johnson, C. C. Gotschalk, and E. T. Egland. 2001. A gas-capture buoy for measuring bubbling gas flux in oceans and lakes. J. Atmos. Ocean. Technol. 18:1411-1420 [doi:10.1175/1520-0426(2001)018<1411:AGCBFM>2.0.CO;2].

Wilson, J. O., P. M. Crill, K. B. Bartlett, D. I. Sebacher, R. C. Harriss, and R. L. Sass. 1989. Seasonal variation of methane emissions from a temperate swamp. Biogeochemistry 8:55-71 [doi:10.1007/BF02180167].

Submitted 11 November 2009
Revised 5 April 2010
Accepted 13 May 2010